CrossMark

Control strategy of twist springback for aluminium alloy hybrid thin-walled tube under mandrel-rotary draw bending

Xin Xue [1,2] · Juan Liao [1] · Gabriela Vincze [2] · António B. Pereira [2]

Abstract The focus of this work is to investigate the control strategy of twist springback of an industrial aluminium alloy extruded tube after mandrel-rotary draw bending, which is a complex nonlinear physical process with coupling multi-factor interactive effects. A particularly pronounced twist springback characteristic of an AA6060-T4 hybrid thin-walled bent tube was observed. It leads to difficulty at the assembly stage due to the inaccurate geometry of product. For an accurate modelling of material behaviours, a non-quadratic anisotropic yield criterion integrated with combined isotropic and kinematic hardening model was adopted to describe the strain-stress behaviours including anisotropy, Bauschinger effects and permanent softening. The corresponding mechanical tests, e.g., enhanced forward-reverse simple shear tests, were performed to identify the material parameters. By using the improved and validated finite element model, two process control strategies related to the mandrel nose placement and the axial push assistant loading are proposed for the assessment of the control efficiency. The simulation results indicate that the mandrel nose placement mainly affects the longitudinal angular springback but not twist deformation in the circumferential sections. The angular springback angle firstly increases and then decreases after several tests of

forward mandrel nose placement. The other control strategy, additional axial push assistant loading with high boost, is able to reduce twist deformation, but the compensation of angular springback is not attained and even a slight increase is observed. It also leads to the rise of the of wrinkle tendency in the intrados sidewall. Finally, the wipe die rake is put forward to reduce the wrinkle tendency due to the high boost applied for twist control.

Introduction

Thin-walled tube bending has attracted increasing applications in many industries to provide an appropriate, cost effective method to replace welded joints used in tricycle production. In the majority of applications, circular tubes are bent because the axisymmetric geometry of the part helps reduce cross-sectional distortion [1]. However, in practice, many industrial structures like rollover protection, frameworks and bumpers usually require bending hybrid thin-walled (HTW) tubes, which contain a mixture of closed and open sections. Aluminium alloy HTW tubes have been extensively used due to the advantages of lightweight, a high bending rigidity and a good flexibility in assemblage.

Among various tube bending methods, mandrel-rotary draw bending (MRDB) has become one of advanced and universal ways to form thin-walled bent tube components with complex cross-sectional shape [2]. It is a multi-die interaction physical process with multifactor coupling effect and multiple defects such as local wrinkling [3], over thinning [4], cross-section distortion [5–7] and springback [8–14] in terms of individual case. The interactions

✉ Juan Liao
jliao@fzu.edu.cn; jliao@ua.pt

1 School of Mechanical Engineering and Automation, Fuzhou University, Fuzhou, Fujian 350116, China

2 Centre for Mechanical Technology and Automation, Department of Mechanical Engineering, University of Aveiro, 3810-193 Aveiro, Portugal

between local buckling and elastic springback in forming of thin-walled aluminium extrusions was investigated by means of numerical and experimental methods [15]. From the view of the material studied, recently, the bending behaviours of large diameter thin-walled CP-Ti tube in rotary draw bending (RDB) was investigated by Zhang et al. [4]. The thin-walled rectangular H96 brass tube under RDB was studied by Zhu et al. [16, 17] as well as the effects of process parameters and the multi-parameter sensitivity degrees on springback and section deformation. Li et al. [10] indicated that the material properties (Young's modulus, strength coefficient and anisotropy coefficient) and the geometrical dimensions dominate the unloading, and the springback values of the high strength Ti-tube (HSTT) are far larger than the ones of the 5052-O Al-alloy tube and the 1Cr18Ni9Ti tube. Liao et al. [11] and Xue et al. [12] investigated the twist springback phenomenon and elastic-plastic deformation mechanism of an AA6060 thin-walled tube with asymmetric section in MRDB.

In this work, the authors focus on the aluminium alloy HTW structures, of which the undesirable twist springback phenomenon is inevitable due to geometric asymmetry, nonlinear material behaviours, unbalanced elastic-plastic deformation and residual stress release [12, 14]. This leads to difficulty at the assembly stage because of the inaccurate geometry of product. The twist springback includes two main modes of deformation behaviours. In the longitudinal direction, the amount of springback can be expressed as the value of bending angle recovery. In the circumferential direction (cross sections), the amount of twist can be denoted by the warping angle of open section (fin). It is not an easy/simple task to calculate twist springback through analytical models. This is because it involves geometric nonlinearities, intricate interfacial conditions and complex material behaviours. Although analytic models [13, 18, 19] or semi-analytical ones [8, 20] for 2D springback has already been developed, the numerical approach by finite element (FE) modelling appears to be the most viable way for deformation analysis and control strategy of twist springback.

In the past decade, many considerable studies have been devoted to accurate prediction of springback of MRDB by finite element modelling [16, 17, 21], rather less attention has been paid to the more complicate twist springback and its control strategy. In practice, the efficient control of the twist springback is vital in precision manufacturing and still treated by the know-how experience and "try and error" tests [22, 23]. Welo et al. [24] developed an adaptive forming technology with automated closed-loop feedback control strategy. By activating this method, the dimensional accuracy of the bent parts is more than three times better than that obtained by traditional compression bending [25]. Furthermore, the concept of flatness limit curves was

introduced as a new, visual Design-for-Manufacturing (DFM) tool aimed to leverage more knowledge based decisions within multi-disciplinary product engineering teams [26]. Li et al. [27] indicated that the mandrel parameters have more obvious influence on the bending quality for the large diameter thin-walled aluminium alloy tubes than for the small diameter thin-walled tubes. Bardelcikand and Worswick [28] attempted to experimentally apply the increased boost to reduce the major strain. Their results indicated that the major strain distribution and the thinning at the outside of the bend are reduced while the inside of the bend thickens with increasing boost. Engel and Hassan [29] investigated the effect of the neutral axis shifting on the strain, wall thinning and thickening. The above efforts provide a trigger on the investigation of the effects of axial force for twist springback control occurring in MRDB.

The objective of this paper is to identify ways to control the twist springback for lightweight automotive structures subjected to mandrel-rotary draw bending. It involves experiments, numerical modelling and elastic-plastic deformation analysis to answer to the following three questions: First, how do the important process factors affect twist springback? Second, what are the interaction between twist springback and other potential defects (e.g., wrinkle); Third, is there any efficient control strategy to minimize twist springback of bent complex structures? In this work, by using the improved FE model of MRDB, the control strategies related to two key process parameters, i.e., the mandrel nose placement and the push assistant loading with boost, are assessed for the efficient reduction of twist springback of an industrial HTW bent tube, as shown in Fig. 1. The effects of wipe die rake on wrinkle and twist springback are also analysed and discussed. These FEA-based control strategies should be helpful to establish robust tool design and forming condition for stable and precise manufacturing of lightweight structures with complex cross-sectional shape.

Modelling procedures

Constitutive model

For the preparation of AA6060-T4 HTW tube, it was provided in the as-received state. The extruded AA6060 profile were cooled by water quenching, straightened by tractioning up to approximately 2% overall strain and naturally aged at room temperature to a substantially stable condition (more than 12 h). Temper T4 exhibits cyclic hardening, and the degree of cyclic hardening depends on the strain amplitudes and the prior strain history [30]. This is why the non-linear kinematic hardening rule should be adopted to model the evolution of cyclic hardening or softening. Some previous works indicate that the

Fig. 1 Twist springback characteristics of a hybrid thin-walled tube after mandrel-rotary draw bending

AA6060-T4 HTW bent tube

Twist springback
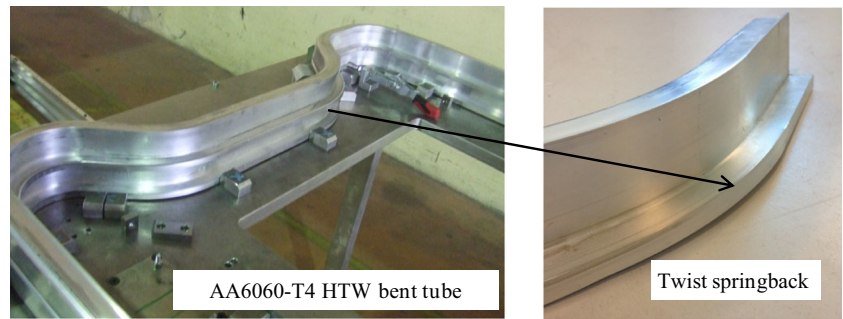
studied material AA6060-T4 exhibits a significant plane anisotropy [30–32] as well as Bauschinger effect and permanent softening during reverse loading [11, 12]. Therefore, the Yld2000-2d anisotropic yield criterion [33] integrated with combined isotropic and kinematic hardening (IHKH) model [34] was adopted in order to represent such behaviours appropriately. While details are referred to the two original papers, the constitutive models are briefly summarized here.

Yld2000-2d yield criterion

In order to describe the anisotropic yield stress surface, the non-quadratic plane stress yield function Yld2000-2d yield criterion proposed by Barlat et al. [33] is employed and given by

$$\phi = \left[\frac{1}{2} \left(\left| \tilde{s}_1' - \tilde{s}_2' \right|^a + \left| 2\tilde{s}_2'' + \tilde{s}_1'' \right|^a + \left| 2\tilde{s}_1'' + \tilde{s}_2'' \right|^a \right) \right]^{1/a} \quad (1)$$

where a is a material coefficient associated to the crystal structure, $\tilde{s}_i'$ and $\tilde{s}_i''$ ($i = 1, 2$) are the principal values of $\tilde{\mathbf{s}}' = \mathbf{L}' \boldsymbol{\sigma}$ and $\tilde{\mathbf{s}}'' = \mathbf{L}'' \boldsymbol{\sigma}$, which are written in tensor notation with the stress deviator $\mathbf{s}$ and the stress tensor $\boldsymbol{\sigma}$. $\mathbf{L}'$ and $\mathbf{L}''$ contain a total of eight anisotropy coefficients α_k, which can be obtained by the corresponding mechanical experiments. The products of these two transformations can be expressed in matrix form as below

$$\left[\mathbf{L}'\right] = \begin{bmatrix} L_{11}' & L_{12}' & 0 \\ L_{21}' & L_{22}' & 0 \\ 0 & 0 & L_{66}' \end{bmatrix} = \frac{1}{3} \begin{bmatrix} 2\alpha_1 & -\alpha_1 & 0_1 \\ -\alpha_2 & 2\alpha_2 & 0 \\ 0 & 0 & 3\alpha_7 \end{bmatrix},$$

$$\left[\mathbf{L}''\right] = \begin{bmatrix} L_{11}'' & L_{12}'' & 0 \\ L_{21}'' & L_{22}'' & 0 \\ 0 & 0 & L_{66}'' \end{bmatrix} = \frac{1}{9} \begin{bmatrix} 8\alpha_5 - 2\alpha_3 - 2\alpha_6 + 2\alpha_4 & 4\alpha_6 - 4\alpha_4 - 4\alpha_5 + \alpha_3 & 0 \\ 4\alpha_3 - 4\alpha_5 - 4\alpha_4 + \alpha_6 & 8\alpha_4 - 2\alpha_6 - 2\alpha_3 + 2\alpha_5 & 0 \\ 0 & 0 & 9\alpha_8 \end{bmatrix} \quad (2)$$

The eight anisotropy coefficients α_k can be determined from standard uniaxial tension tests in the rolling, transverse and diagonal directions and equi-biaxial tension tests. The calculation of coefficients requires a numerical optimisation solver, e.g., the Newton-Raphson method [35, 36].

Combined isotropic and kinematic hardening model (IHKH)

The whole process of MRDB includes three basic steps: bending tube, retracting mandrel and springback. This means that the deformation path involves the tension and compression stress state in the extrados and intrados side respectively, and forward-reversal loading conditions. Therefore, the combined isotropic and kinematic hardening model, which has proven to be able to capture the Bauschinger effect, was employed. For the constitutive description, a yield surface of first-order homogeneous function is expressed as [34, 37]

$$\phi(\boldsymbol{\sigma} - \boldsymbol{\alpha}) - \overline{\sigma}_{iso} = 0 \quad (3)$$

Here, the back stress $\boldsymbol{\alpha}$ represents the translation of yield surface from the initial position, and the effective yield stress $\overline{\sigma}_{iso}$ measures the size of yield surface. The evolution of $\boldsymbol{\alpha}$ can be expressed by the non-linear kinematic hardening model:

$$d\boldsymbol{\alpha} = C \frac{d\overline{\varepsilon}^p}{\overline{\sigma}} (\boldsymbol{\sigma} - \boldsymbol{\alpha}) - \gamma \boldsymbol{\alpha} d\overline{\varepsilon}^p \quad (4)$$

where $\boldsymbol{\sigma}$ and $d\overline{\varepsilon}^p$ denote the Cauchy stress tensor and the equivalent plastic strain, $\overline{\sigma}$ is the effective stress and C and γ

are material parameters. C, $\overline{\sigma}$ and γ determine the plastic hardening rate following an abrupt change of loading path.

During cyclic loading, there also exists the effect of isotropic hardening, e.g., the Voce law:

$$\overline{\sigma} = \sigma_0 + Q\left(1 - e^{-b\overline{\varepsilon}^p}\right) \tag{5}$$

where σ_0 is the initial yield stress, $\overline{\varepsilon}^p$ is the plastic strain after yield state, and Q, b are the material parameters evaluated from best approximation of a uniaxial flow curve.

Mechanical tests and parameter identifications

Simple shear and Bauschinger tests

The planar simple shear (SS) test has proved to be a very efficient technique to evaluate the mechanical properties of flat samples [38]. Especially, Bauschinger effect can be captured through direct and reverse shear tests. Many advantages offered by this technique were introduced by Vincze [39] as well as the construction of the previous shear device. A rectangular shear sample is firmly clamped by the two grips, as shown in Fig. 2a. One of grips is fixed while the other moves along the x-axis. The constant width h of the deformation area is maintained during the test. L and Δx are the current length of the specimen and the relative displacement of the two grips during simple shear deformation, respectively.

The main challenge of SS test is to achieve a robust clamping. As shown in Fig. 2b, c, the entire specimen is encapsulated into the serrated groove with specially designed hatching knurling texture. This design of gripping system is able to well prevent the sample slipping. The depth of the groove is 0.6 mm, the length of the groove 35 mm, the distance between the left and right grips 3.0 mm and the height of texture is 0.45 mm. In order to prevent the rotational rigid motion of the global apparatus in the SS test, the enhanced shear apparatus with 4-guide structure was developed, as shown in Fig. 3. The diameter of each guide pillar is 14 mm.

Note that there were only two guide pillars in the previous shear device.

The simple shear tests were conducted with the universal tensile testing machine SHIMADZU-AG-100kN to characterize the plastic behaviour of material upon reversal loading mode. Monotonic shear test and forward-reverse shear tests with different pre-strain were performed with a strain rate of 10^{-3} s^{-1}. Four samples were performed for each mechanical test to check the consistency and one of them was used as representative. The dimension of the initial rectangular shear sample is 35 mm × 15 mm × 2.0 mm, which has been optimized to achieve a uniform shear strain in the centre area. The shear strain field was obtained by using the digital image correlation (DIC) technique, namely the ARAMIS 5 M. Due to the buckling impact in the both sides of the sample, only the data in the centre area were used for the strain calculation. An appropriate area of interest (AOI: 12.0 × 2.0 mm) was selected, in which the shear deformation is almost uniform (ranges from 25.5° to 26.5°) as shown in Fig. 4.

Material parameter identifications

It is noted above that the material characterization for the Yld2000-2d model requires three standard uniaxial tensile tests at the angles 0°, 45° and 90° with respect to the extruding direction and a test for the equi-biaxial stress state. Due to the geometric limitation of the un-deformed thin-walled tube, the equi-biaxial experiment is not available. The uniaxial stress along the extrusion direction was arbitrarily used instead. Note that the exponent a in the Yld2000-2d model for FCC materials (i.e., AA6060-T4) is taken to be equal to 8.0. The input data of stresses were not the values at yield but those determined at a specific plastic work [40] of 15 MPa, which achieves an adequate plastic deformation. The model parameters of the IHKH model with Yld2000-2d are identified by analytic method and then calibrated by numerical testing. The resulting parameters are listed in Table 1.

The sample tested in simple shear was cut from the extruded tube before bending process. As shown from Fig. 5, the

Fig. 2 (a) Schematic description of the SS test (b) grips with groove and texture design (front view) (c) side view after full clamping
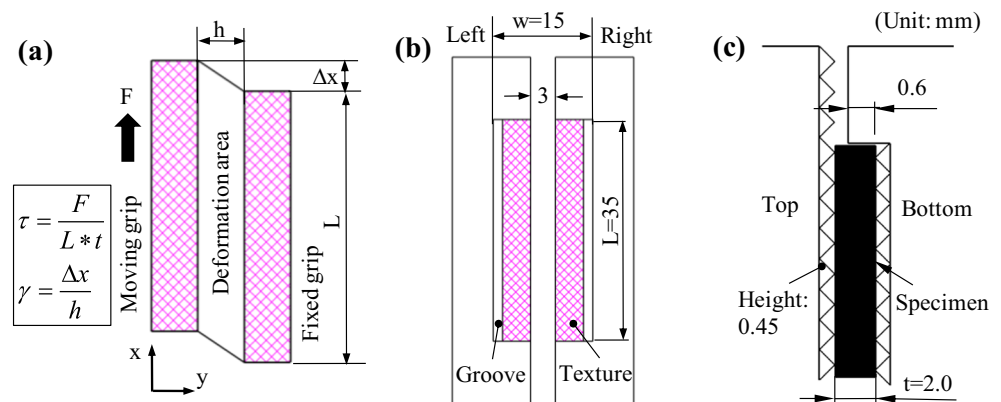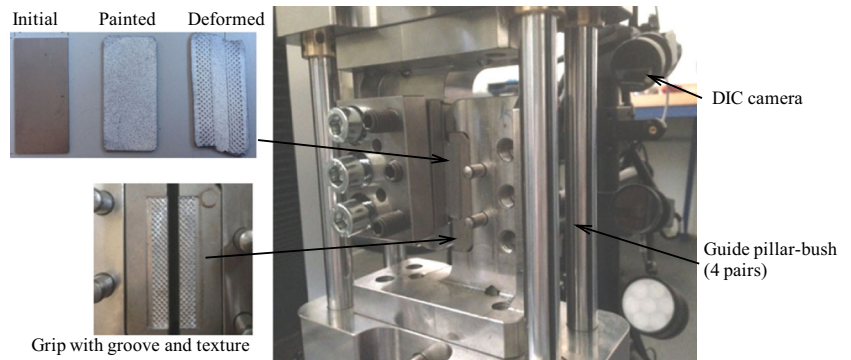
Fig. 3 The enhanced simple shear device

Grip with groove and texture

DIC camera

Guide pillar-bush (4 pairs)

identified curves show that evident difference of the hardening laws occurs in the forward and reverse shear tests. After the load reverse, the IHKH model reproduces the Bauschinger effect and transient behaviour of this material very well whereas the IH model captures neither of them. Although some discrepancies are found in reproducing the curve crossing response [41] by the IHKH model, the whole predicted results by the IHKH model are acceptable. More detailed descriptions on the material parameter identifications and the influence of constitutive models can be referred to the authors' previous work [11].

Finite element modelling and its experimental validation

An improved FE model for mandrel-rotary draw bending process of hybrid thin-walled aluminium alloy tube was established, as shown in Fig. 6. The dynamic-explicit time integration scheme was used for the simulation of the forming process, and implicit time integration for springback. The elastic-plasticity constitutive models described in the previous Section were implemented into ABAQUS through the user subroutines VUMAT/UMAT. The key modelling techniques were consistent with those in the original model in Ref. [12], such as the surface-based coupling HINGE constraint for flexible mandrel and numerical inverse method for interfacial friction coefficient identification. The core of this work will focus on the control strategies by using the developed FE model. However, the fine shell element (1.0 mm × 2.0 mm) has been

adopted for the main deformation area and should make a more precise prediction to springback than the previous coarse mesh element.

The basic forming and geometric parameters are listed in Table 2. Fig. 7 shows the experimental apparatus involved plastic wipe die and multi-bending axis, which has been also used for mass production of the AA6060-T4 HTW automotive structure. The validity of the FE model has been assessed by comparing the predicted twist springback and side wall thinning with the experimental ones in the previous works [12]. The twist springback of studied HTW tube can be decomposed into two main codes of deformation behaviours. In the longitudinal direction, the amount of springback can be expressed as the bending angular change of rectangular close section after the release of residual stress. In the circumferential direction, the amount of twist can be defined as the warping angle of open section. More detailed information on the description of twist springback and the corresponding deformation analysis can be referred to the authors' previous works [11, 12].

Control strategies

In this Section, a special attention is paid to the control strategy of twist springback in mandrel-rotary tube bending, a topic that has not been emphasised often so far. In the authors' prior works [11, 12], from the view of elastic-plastic

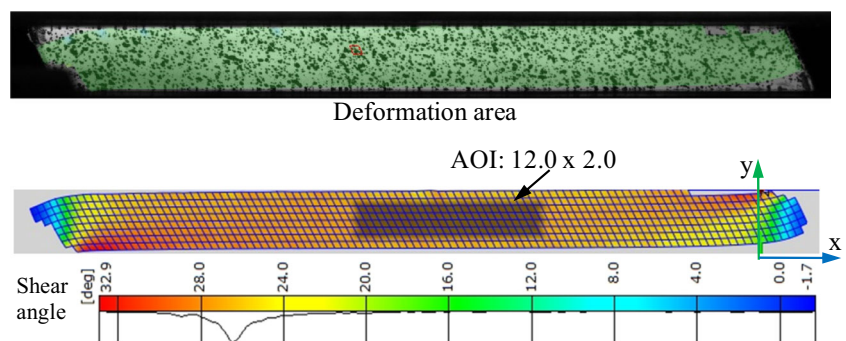**Fig. 4** DIC images of shear deformation

Deformation area

AOI: 12.0 x 2.0

Shear angle [deg]

Table 1 Material parameters of AA6060-T4 for the constitutive models used

Anisotropy	σ_0/σ_0	σ_0/σ_{45}	σ_0/σ_{90}	σ_b/σ_0	r_0	r_{45}	r_{90}	r_b	
	1	0.843	0.929	1	0.492	0.367	1.277	0.353	
Yld2000-2d	α_1	α_2	α_3	α_4	α_5	α_6	α_7	α_8	α
	0.766	1.266	0.751	0.975	1.052	1.070	0.871	1.592	8
IHKH	σ_0 (MPa)	Q (MPa)	b	C (MPa)	γ				
	86.4	137.5	6.74	3221.2	59.6				

deformation mechanism, since the tube undergoes in-plane tensile at the extrados and compressive deformation at the intrados during the bending process, shear deformation may arise in the wall regions. The negative torsion moment can be roughly explained in conjunction with the in-plane shear stress. During the springback process, the flange region at the extrados of the tube that undergoes stretching deformation requires in-plane compression, whereas the intrados of the tube that undergoes shrinking deformation requires in-plane tension. These in-plane deformations have the opposite effect to the first factor during the bending process. Thus, release of the longitudinal tangent stress during springback process will cause positive twist, which will decrease the whole twist deformation in the flange. The previous efforts provide a trigger on the control strategy of twist springback in terms of axial force or longitudinal tangent stress field during the bending process. Therefore, two key process parameters related to axial force, i.e., the mandrel nose placement and the push assistant loading with boost, are assessed for the efficient reduction of twist springback in the present work.

Mandrel nose placement (MNP)

In MRDB, the tube wall will thicken along the inside radius (intrados) and will thin along the outside radius (extrados) as
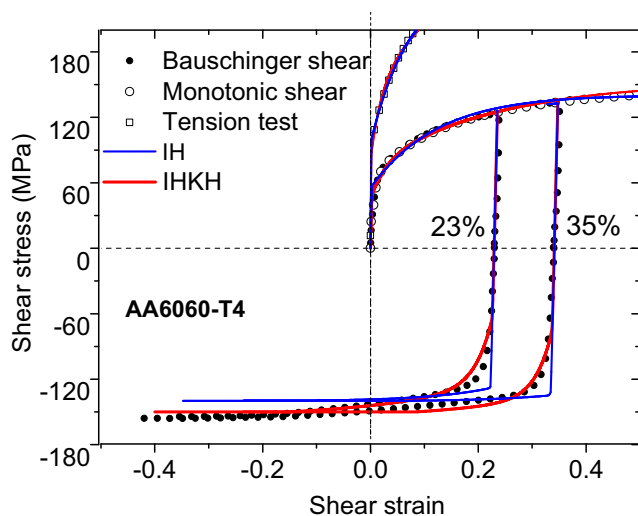

Fig. 5 Comparison of measured and predicted Bauschinger shear stress-strain curves

the clamps draw the tube around the bend die. The purpose of the mandrel nose, as shown in Fig. 8, is to cover this region of flowing material and ensure a consistently round cross section by mitigating the simultaneous compression and stretching of the tube wall.

As one scheme, the mandrel in a too far forward position stretches the material on the outside of the bend more than necessary. This increases the length of material on the outside beyond what is required to make a bend. Fig. 9a is an exaggerated example. Bumps appear on the extrados of the bend and are most evident at the end of bend. A step may begin to appear on the intrados at the start of the bend. On the other hand, the mandrel in a too far back position does not adequately stretch the material on the outside of the bend and generate enough pressure on the inside of the bend to compress the material. This may lead to form a wrinkle or wave on the intrados of the tube, as shown in Fig. 9b. Therefore, the mandrel nose placement (MNP) relative to the point of bend or the line of tangency should affect the stress and deformation state of the bent tube.

In order to identify an analytic value of MNP, some fundamental assumptions are given as follows: 1) the cross-sectional distortion and wall thickness reduction are ignored; 2) the centrelines of mandrel shank and thin-walled tube are collinear; 3) the whole flexible mandrel including mandrel shank and flexible cores is rigid or non-deformable; 4) the edge of mandrel nose is tangent to the inside wall of tube. As illustrated in Fig. 10, the ideal value of MNP can be calculated by using ΔOAB:

$$e = |AB| = \sqrt{|OA|^2 - |OB|^2}$$
$$= \sqrt{\left(R_{CLR} + \frac{W_0}{2} - t\right)^2 - \left(R_{CLR} + \frac{W_1}{2} - r \cdot \sin^2\alpha\right)^2} \quad (6)$$

in which

$$\mu = \frac{W_0 - W_1}{2} - t \quad (7)$$

and for large diameter thin-walled tube
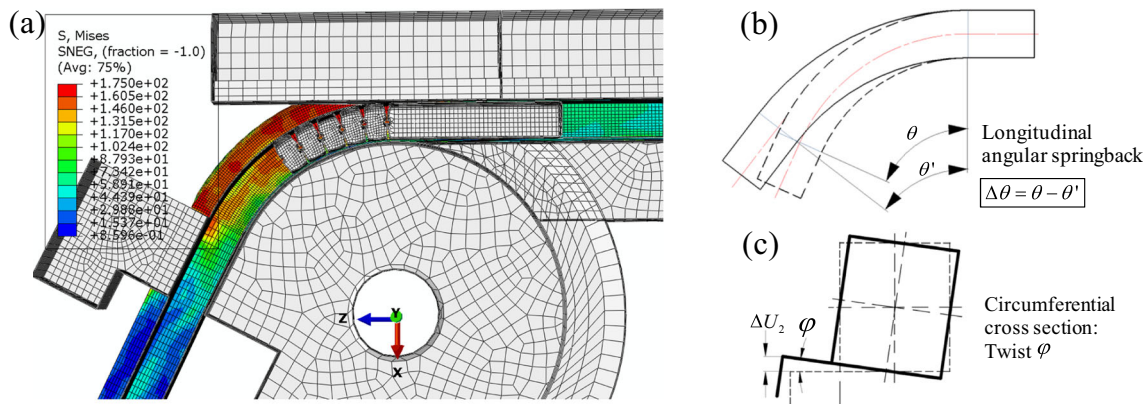
$$r \cdot \sin^2\alpha \approx 0 \quad (8)$$

Fig. 6 (**a**) Finite element model of mandrel rotary draw bending (**b**) longitudinal springback angle (**c**) twist

Hence the ideal value of MNP can be simplified and given by

$$e = \sqrt{2\left(R_{CLR} + \frac{W_0}{2} - t\right) \cdot \mu - \mu^2} \qquad (9)$$

where e, R_{CLR}, t and μ denote the mandrel nose placement, the radius of geometric centre curve, wall thickness and clearance between mandrel and tube, respectively. α, r and W_1 are defined as the sine angle between mandrel nose placement and the extrados radius of interior thin-walled tube, mandrel nose radius and the width of mandrel shank, respectively. W_0 represents the width of extrados thin-walled rectangular tube or outward diameter of circular thin-walled tube. From Eq. (9), it also can be observed that mandrel nose placement is irrelevant to the bending angle. This means that MNP can be a constant for multiple bent tubes.

Push assistant loading (PAL)

In order to improve the thin-walled tube bendability and mitigate the residual stress in the longitudinal direction, generally, the pushing tools including the movable pressure die or booster could be used to provide the push assistant loading (PAL) for MRDB. How to determine the appropriate PAL plays an important role for the control of twist springback and other deformation behaviours.

As shown in Fig. 11, the pressure die exerts the axial friction force to the outside of tube. This axial compressive force counteracts the drag force done by the inside mandrel/wiper die and helps push the materials past the tangent point and into the bending regions. It decreases the tensile stress and makes the strain neutral line (NL) shift outwards, as illustrated in Fig. 12. In a normal process, the pressure die displaces the same distance as the arc length that is swept by the centre-line radius (CLR). This is referred to as the "medium boost" case where the ratio of the displacements is 100%. By changing the displacement of the pressure die relative to the arc length swept by the CLR of the bend die, the calculation for pressure die boost is given by

$$P_L = \frac{L_P}{L_{CLR}} \times 100\% = \left(1 + \frac{360 W_0}{\pi R_{CLR} \theta}\right) \times 100\% \qquad (10)$$

Table 2 Forming parameters of MRDB and friction coefficients on various tube-die interfaces

| Forming conditions		Friction conditions		
Process parameters	Values	Interfaces	Lubricants	Inverse values
Bending velocity, ω/(rad·s)	0.523	Tube-bend die	Dry	0.1
Bend angle, θ/(°)	45	Tube- pressure die	Dry	0.38
Centreline radius, R_{CLR}/(mm)	130	Tube- mandrel	Mineral oil	0.08
Speed of pressure die, V_p(mm/s)	60	Tube- wiper die	Dry	0.15
Clearances between tube and tools (mm)	0.1	Tube-clamp die	Tough dry	rough
Speed of mandrel retracted, V_m (mm/s)	100	Note1: Lubricate oil is IRMCO GEL 980–000.		
Mandrel flexible cores	5	Note2: Coulomb friction law.		
Length of pressure die, L_p (mm)	210			
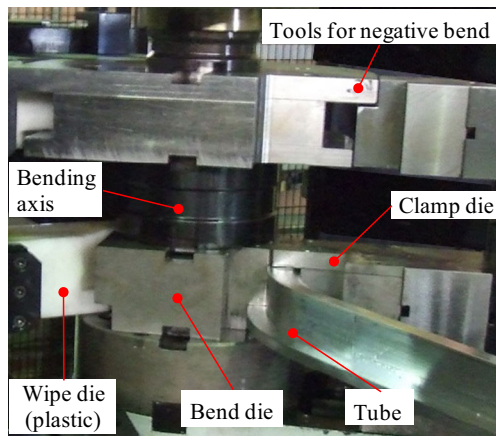
Fig. 7 Experimental tools with a plastic wipe die and a multi-bending axis

in which

$$L_P = L_{CLR} + 2W_0, L_{CLR} = \frac{\pi R_{CLR}\theta}{180} \tag{11}$$

where L_P and L_{CLR} are the length of pressure die and the theoretical centreline arc length respectively. θ represents the bending angle. According to Li et al. [3], $2W_0$ (2 times of the tube diameter or width W_0) is the needed length for resisting the warping relative to the rigidity of the tube material. Here, this empirical value is considered as the "positive boost" from pressure die. Additionally, the other possible scheme is to change the push assist speed of pressure die for the improvement of axial force. However, it is limited since it should be compatible to the bending speed of bend die.

To ensure the above "positive boost" was achieved without the tube slipping relative to the pressure die, a boost collet can be used to couple the end of the tube to the pressure die. Moreover, the booster, one of the movable pushing tools, can be also used to apply the axial boosting force to control the flow
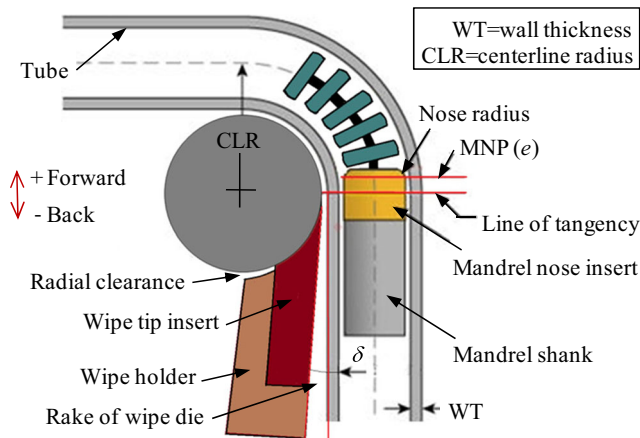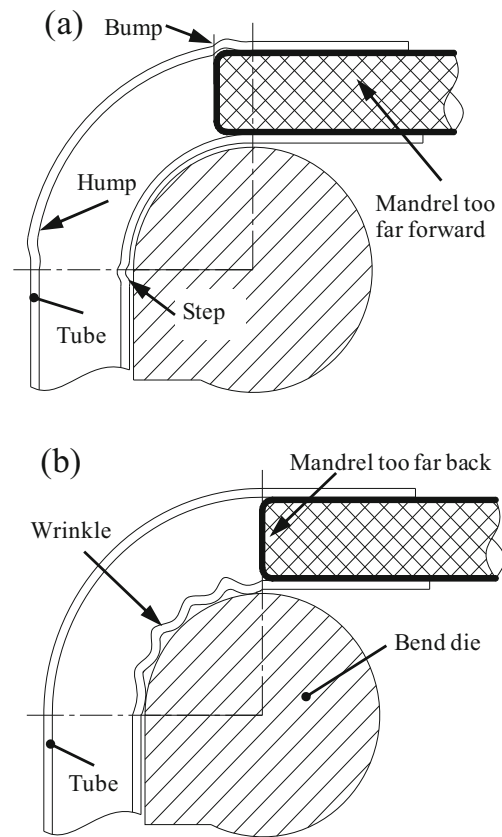

Fig. 9 (a) The mandrel in a too far forward position (b) the mandrel in a too far back position

state of tube materials. Fig. 11 also shows that there are five possible methods to apply the axial boosting force via booster:

(a) To provide the push assistant force directly at the trailing end of tube;
(b) To provide the push assistant force by the friction between booster and outer surface of tube;
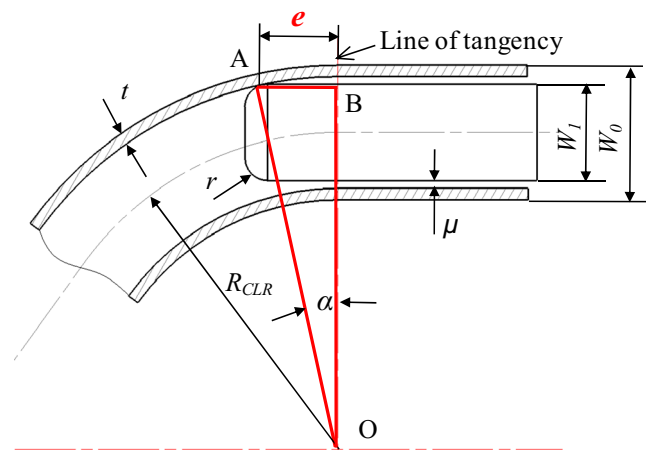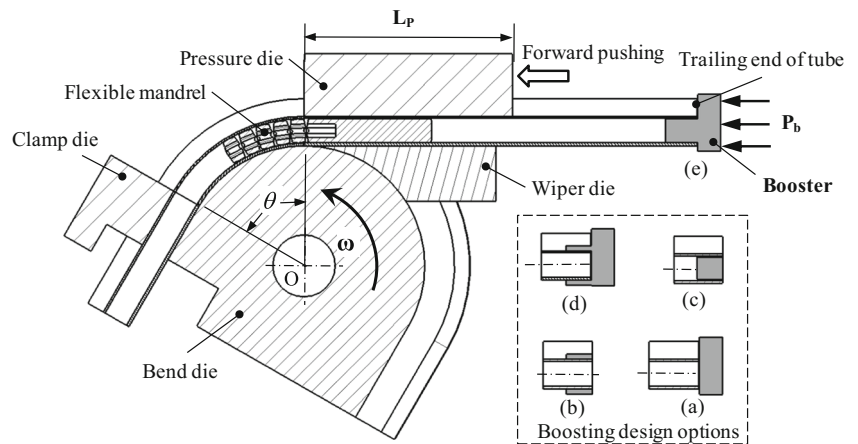(c) To combine the above two boosting methods to exert the boosting force;

Fig. 8 Illustration of mandrel nose placement and wipe die rake in MRDB

Fig. 10 The geometries of MNP

Fig. 11 Sketch of boosting design options for push assistant loading in MRDB

(d) To provide the push assistant force by the friction between booster and inner surface of tube;

(e) To combine the first method and the fourth one to boost the tube. To evaluate the efficiency of the boosting method on springback control of thin-walled tube, the last boosting method with respect to different boosting force conditions was adopted based on the developed FE model.

The previous researches [3] have tended to use a nominal index of the booster assistant level associated with the speed ratio of the booster and centreline bender. It can be expressed as

$$f_b = \frac{V_b}{V_{CLR}} \times 100\%, \text{ with } V_{CLR} = \omega \cdot R_{CLR} \quad (12)$$

where V_b and V_{CLR} are the speeds of booster and the instant tangential linear speed measured at the centreline bending radius of bend die, respectively. ω represents the angular velocity of the bending die.

This push assistant level related to forming speed may be a good matching mode for PAL. However, in this work, the authors prefer to directly apply the booster force or axial pressure at the trailing end of tube. It can be implemented by adding a simple device in the CNC machine with a particular spring, which can provide the designate value of axial force on the tube during the forming process. It is worth to note that both PAL methods might induce the local wrinkling due to simultaneously induced excessive compressive stress at the

intrados of tube. Thus it is necessary to study the interactive effects of PAL conditions on different defects such as wrinkling, wall thinning and cross-section deformation.

Results and discussions

The effect of MNP on twist springback

In order to study the effect of MNP on twist springback, several levels of forward MNP were introduced into the FE model and tested the feasibility for the control of twist springback. According to Eq. (9) and the geometry of the HTW tube, the theoretic value of MNP, i.e., 5.69 mm, can be obtained. Hence, the range of the tested MNP change can be from 0 to 10 mm, and there are almost no other undesirable defects mentioned above. Fig. 13 shows the comparison of the predicted twist springback by using different MNP in the case of 45° bending thin-walled tube. It can be observed that the angular springback slightly increases at first and then decreases after 6.0 mm. This might be because the first increase of MNP aggravates the large deformations on the extrados side including the rate of elastic deformation, which leads to the larger angular springback. The further increase of MNP may mitigate the intrados compression deformation and then cause the decrease of angular springback. The MNP should also make an important effect on the ovalisation or distortion of the close

Fig. 12 Stress distribution and strain neutral line change of the cross-section of bending tube under PAL conditions
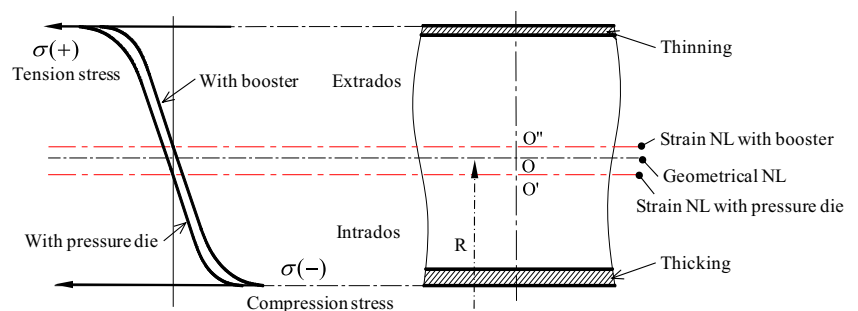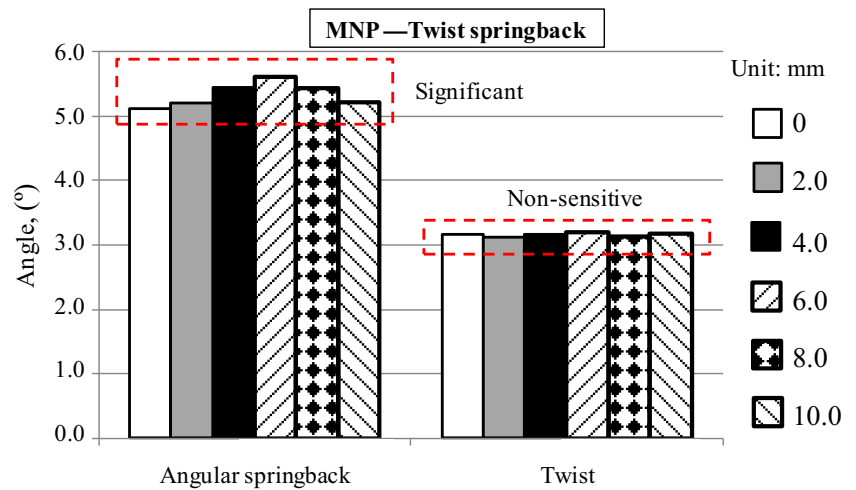
Fig. 13 Comparison of twist springback calculated by using different tested MNP

section, but it is not significant in this particular case. For the twist deformation in the flange, no remarkable difference has been observed between the situations. This might be because, for the particular HTW structure, there is no directly interfacial contact between flexible mandrel and the open section part, which is the place of twist occurrence.

The effect of PAL on twist springback

Nowadays, many newer CNC tube-bending machine have both "assist" pressure and "boost" pressure. The term "boost" generally means a type of axial pressure applied during the bend to the entire circumference of the tube by means of clamps behind the pressure die. By using this type of pressure force, deformable material passes through the line of tangency to feed both the intrados and the extrados. Assist, on the other hand, feeds material only into the extrados which is useful in decreasing flattening and wall-thinning. In this work, to test the effect of PAL on twist springback, several virtual levels of axial pressure or "boost" were applied on the trailing end of

the thin-walled tube during the MRDB. The range of high boost is from 0.3 MPa to 0.9 MPa with an interval of 0.2 MPa. Fig. 14 compares the maximum twisting and springback angles calculated by using different PAL conditions. It can be observed that 23.5% degradation of twisting deformation can be achieved by 0.9 MPa PAL condition compared to no PAL condition. However, the compensation of springback of bending angle is not attained and even a slight increase is observed. This is because the PAL mainly be helpful to reduce the longitudinal tensile stress field on the extrados side, rather than the bending moment of the whole section.

By using different PAL conditions, the selected intrados and extrados sidewall thickness distributions were calculated and compared in Fig. 15. The thickness of intrados sidewall increases with the increase of push assistant pressure, while that of extrados sidewall decreases. This means that the extrados sidewall has less deformation, but the tendency of the wrinkle in the intrados sidewall rises.

Although the proposed PAL method with boost has proved to be efficient for the reduction of twist deformation of the

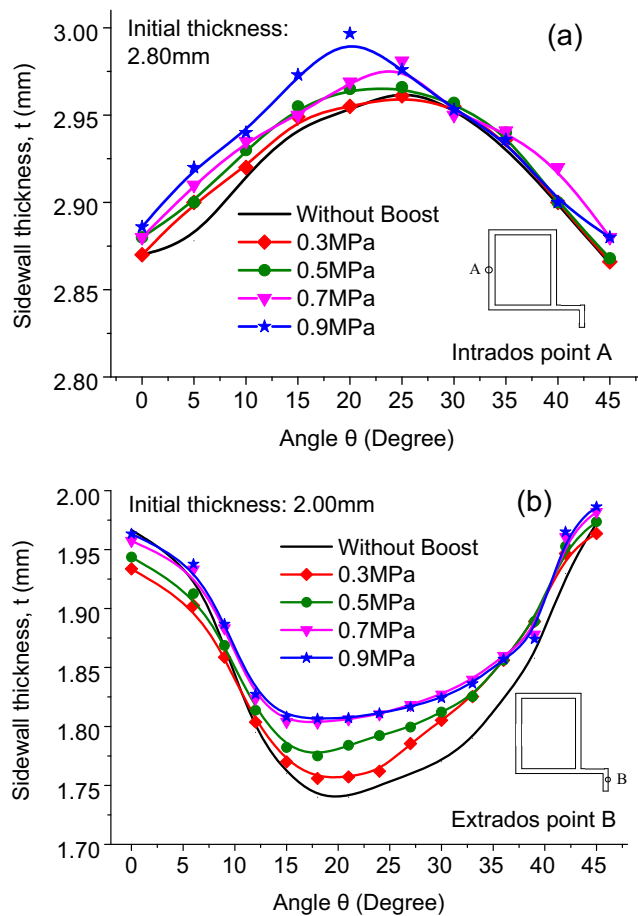**Fig. 14** Comparison of twist springback calculated by different PAL conditions
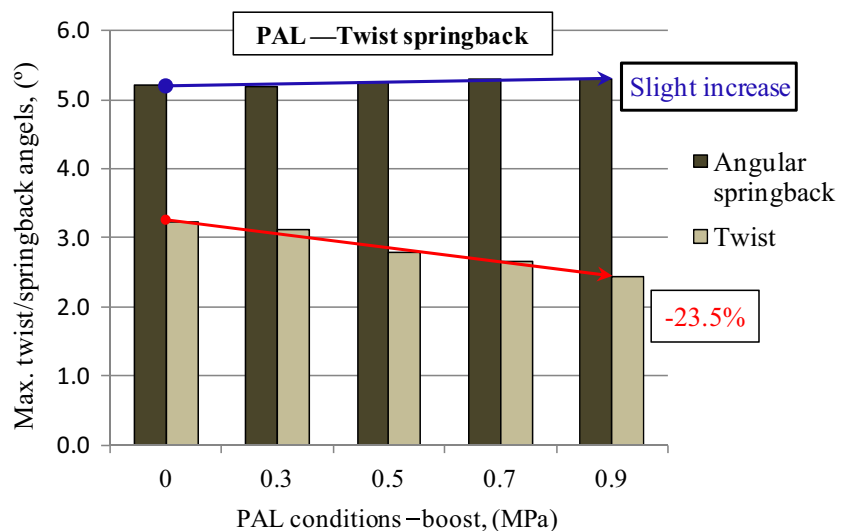
Fig. 15 Comparison of the sidewall thickness distributions calculated by using different PAL conditions: (**a**) intrados (**b**) extrados

presented case, the authors think this alternative approach still needs to be tested in more other possible industrial applications. It should be of particular significance for the forming processes with obvious axial force.

The effect of wipe die rake on twist springback and wrinkle

In order to balance the twist control and wrinkle occurrence, a wiper tip properly raked from the line of tangency, as shown in Fig. 8, is proposed to prevent the wrinkle or series of small wrinkles that can form at the terminal end of the intrados bent tube. Theoretically, the wiper die including wiper tip insert and wiper die holder fills the gap behind the line of tangency the inside line of the tube and the curve of the bend die cavity. As the tube is drawn through the line of tangency, the forming material will bulge outward to fill this gap if it is not sufficiently rigid. And this bulge can flatten out between the bend die cavity and the mandrel nose with enough direct pressure-die pressure. However, if the bulge extends far enough to exceed the elasticity of the forming material at the terminus of the

bend, it will not be drawn through or flattened and then form a wrinkle. Therefore, the wiper tip needs to obstruct only that marginal bulging which exceeds the material's elasticity and would set the entire bulge into a permanent wrinkle. This is why a wiper can be raked away from the line of tangency. In addition, it should be noted that the feathered edge of wipe die can approach, but not go past the line of tangency.

In this work, three different levels of the wipe die rake, i.e., $\delta = 0°, 1°, 2°$, with maximum MNP and "high boost", were tested to evaluate its effect on wrinkle and twist deformation of the analysed HTW tube. Fig. 16a indicates that there is a significant reduction of intrados wall thickness or the wrinkle tendency by means of wipe die rake. But there is no remarkable difference observed with the increase of wipe die rake from 1° to 2°. Additionally, Fig. 16b compares the predicted twist springback under different wipe die rake. It is almost no remarkable change. This means that the wipe die rake makes little effect on twist springback. The experimental validation of the wipe die rake on wrinkle firstly was to use a plastic wipe
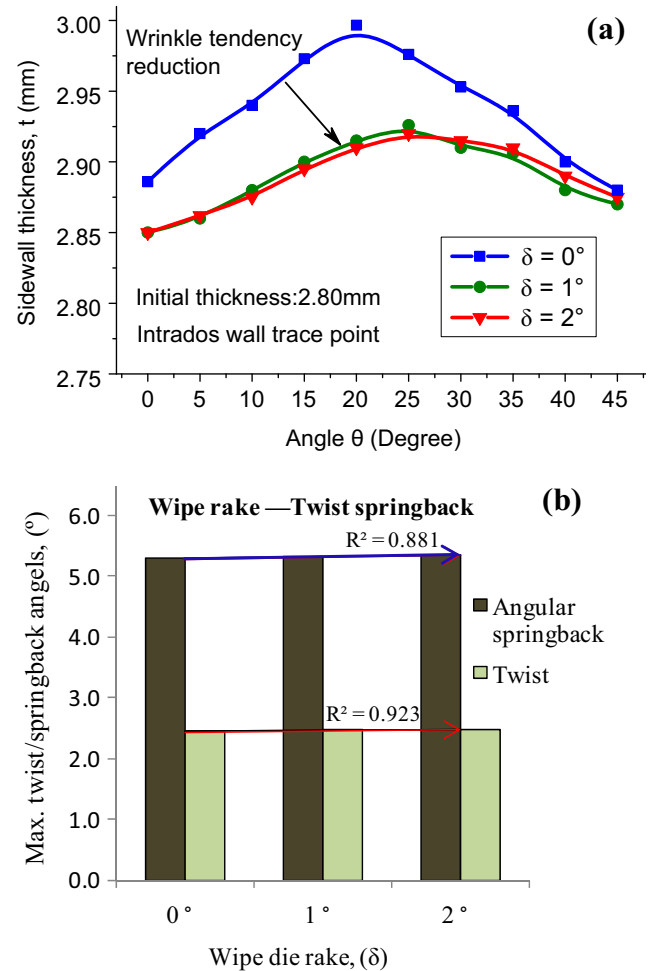

Fig. 16 The effects of wipe die rake on (**a**) intrados sidewall thickness distributions (**b**) twist springback

die. It is an engineering resin (also known as "metal-like") with mechanical properties that make it useful for the prototyping and manufacture of laboratory apparatus, namely Polyoxymethylene (POM) [42]. The experimental observation is in good qualitative agreement with the simulation-based analyses mentioned above. In a word, integrated optimisation of process parameters associated with "Forward MNP", "High boost" and an appropriate wipe die rake should be an efficient control strategy to minimize the twist springback of HTW tube subjected to MRDB.

Conclusions

In this work, the control strategy of twist springback phenomenon for an industrial hybrid thin-walled tube under mandrel-rotary draw bending was investigated by means of numerical method and deformation analysis. By using the developed FE model, the optimization of mandrel nose placement and the application of push assistant loading with boost were to assess the efficiency for the control of twist springback as well as the wipe die rake for the reduction of wrinkle. The principal conclusions are as follows:

1) The mandrel nose placement mainly affects the springback but not twist deformation in the case of presented hybrid thin-walled tube.
2) The push assistant loading with boost is able to reduce twist deformation, but the tendency of springback of bending angle and wrinkle in the intrados sidewall also rises.
3) The wipe die rake provides an efficient control strategy for the wrinkle in the intrados side but not for the twist springback in the extrados side.
4) Interactive effects between twist springback and other deformation defects should be taken into account in the future work and real industrial application.
5) The presented FEA-based control strategies should be helpful to establish robust tool design and forming condition for stable and precise manufacturing of lightweight automotive structures.

Compliance with ethical standards

Conflict of interest The authors declare that they have no conflict of interest.

References

1. Ancellotti S, Benedetti M, Fontanari V, Slaghenaufi S, Tassan M (2016) Rotary draw bending of rectangular tubes using a novel parallelepiped elastic mandrel. Int J Adv Manuf Tech 85:1089–1103
2. Yang H, Li H, Zhang ZY, Zhan M, Liu J, Li GJ (2012) Advances and trends on tube bending forming technologies. Chinese J Aeronaut 25:1–12
3. Li H, Yang H, Zhan M, Kou YL (2010) Deformation behaviors of thin-walled tube in rotary draw bending under push assistant loading conditions. J Mater Process Technol 210:143–158
4. Zhang ZY, Yang H, Li H, Ren N, Tian YL (2011) Bending behaviors of large diameter thin-walled CP-Ti tube in rotary draw bending. Prog Nat Sci Mat Int 21:401–412
5. Paulsen F, Welo T (2001) Cross-sectional deformations of rectangular hollow sections in bending: part I - experiments. Int J Mech Sci 43:109–129
6. Paulsen F, Welo T (2001) Cross-sectional deformations of rectangular hollow sections in bending: part II - analytical models. Int J Mech Sci 43:131–152
7. Zhao GY, Liu YL, Yang H, Lu CH (2010) Cross-sectional distortion behaviors of thin-walled rectangular tube in rotary-draw bending process. Tran Nonferrous Met Soc China 20:484–489
8. Zhan M, Yang H, Huang L (2006) A numerical-analytic method for quickly predicting springback of numerical control bending of thin-walled tube. J Mater Process Technol 22:713–720
9. Jiang ZQ, Yang H, Zhan M, Xu XD, Li GJ (2010) Coupling effects of material properties and the bending angle on the springback angle of a titanium alloy tube during numerically controlled bending. Mater Des 31:2001–2010
10. Li H, Yang H, Song FF, Zhan M, Li GJ (2012) Springback characterization and behaviors of high-strength Ti–3Al–2.5V tube in cold rotary draw bending. J Mater Process Technol 212:1973–1987
11. Liao J, Xue X, Lee MG, Barlat F, Gracio J (2014) On twist springback prediction of asymmetric tube in rotary draw bending with different constitutive models. Int J Mech Sci 89:311–322
12. Xue X, Liao J, Vincze G, Gracio J (2015) Modelling of mandrel rotary draw bending for accurate twist springback prediction of an asymmetric thin-walled tube. J Mater Process Technol 216:405–417
13. Zhan M, Wang Y, Yang H, Long H (2016) An analytic model for tube bending springback considering different parameter variations of Ti-alloy tubes. J Mater Process Technol 236:123–137
14. Sitar M, Kosel F, Brojan M (2015) Numerical and experimental analysis of elastic–plastic pure bending and springback of beams of asymmetric cross-sections. Int J Mech Sci 90:77–88
15. Welo T, Paulsen F (1996) Local flange buckling and its relation to elastic springback in forming of aluminium extrusions. J Mater Process Technol 60(1):149–154
16. Zhu YX, Liu YL, Yang H, Li HP (2012) Improvement of the accuracy and the computational efficiency of the springback prediction model for the rotary-draw bending of rectangular H96 tube. Int J Mech Sci 66:224–232
17. Zhu YX, Liu YL, Li HP, Yang H (2013) Springback prediction for rotary-draw bending of rectangular H96 tube based on isotropic mixed and Yoshida Uemori two surface hardening models. Mater Des 47:200–209
18. Tang NC (2000) Plastic-deformation analysis in tube bending. Int J Press Vessel Pip 77:751–759
19. Al-Qureshi HA, Russo A (2002) Spring-back and residual stresses in bending of thin-walled aluminum tubes. Mater Des 23(2):217–222
20. Zhang ZK, Wu JJ, Guo RC, Wang MZ, Li FF, Guo SC, Wang YA, Liu WP (2016) A semi-analytical method for the springback prediction of thick-walled 3D tubes. Mater Des 99:57–67

21. Zhao GY, Liu YL, Yang H, Lu CH, Gu RJ (2009) Three-dimensional finite-elements modelling and simulation of rotary-draw bending process for thin-walled rectangular tube. Mater Sci Eng A 499:257–261

22. Li H, Yang H, Zhang ZY, Li GJ, Liu N, Welo T (2014) Multiple instability-constrained tube bending limits. J Mater Process Technol 214:445–455

23. Schilp H, Suh J, Hoffmann H (2012) Reduction of springback using simultaneous stretch-bending processes. Int J Mater Form 5:175–180

24. Welo T, Granly B (2010) A new adaptive bending method using closed loop feedback control. Trans Nonferrous Met Soc China 20(11):2111–2117

25. Welo T, Sætertrø K, Søvik OP (2008) Adaptive bending of aluminium extrusions using an automated closed-loop feedback approach. Int J Mater Form 1:197–200

26. Welo T (2014) Design for dimensional accuracy in bending operations: Introducing the concept of flatness limit curves. Proceedings of the ASME 2014 International Design Engineering Technical Conferences & Computers and Information in Engineering Conference IDETC/CIE 2014, August 17–20, 2014, Buffalo, New York, USA

27. Li C, Yang H, Zhan M, Xu XD, Li GJ (2009) Effects of process parameters on numerical control bending process for large diameter thin-walled aluminum alloy tubes. Tran Nonferrous Met Soc China 19:668–673

28. Bardelcikand A, Worswick MJ (2005) The effect of element formulation on the prediction of boost effects in numerical tube bending. Aip Conf Proc 778:774–780

29. Engel B, Hassan HR (2014) Investigation of neutral axis shifting in rotary draw bending processes for tubes. Steel Res Int 85(7):1209–1214

30. Hopperstad OS, Langseth M, Remseth S (1995) Cyclic stress-strain behaviour of alloy AA6060, part I: uniaxial experiments and modelling. Int J Plast 11(6):725–739

31. Hopperstad OS, Langseth M, Remseth S (1995) Cyclic stress-strain behaviour of alloy AA6060, part II: biaxial experiments and modelling. Int J Plast 11(6):741–762

32. Khadykoa M, Dumoulin S, Cailletaud G, Hopperstad OS (2016) Latent hardening and plastic anisotropy evolution in AA6060 aluminium alloy. Int J Plast 76:51–74

33. Barlat F, Brem JC, Yoon JW, Chung K et al (2003) Plane stress yield function for aluminium alloy sheets—part I: theory. Int J Plast 19:1297–1319

34. Chung K, Lee MG, Kim DY, Kim CM, Wenner ML, Barlat F (2005) Spring-back evaluation of automotive sheets based on isotropic-kinematic hardening laws and non-quadratic anisotropic yield functions part I: theory and formulation. Int J Plast 21:861–882

35. Lee JW, Lee MG, Barlat F (2012) Finite element modelling using homogeneous anisotropic hardening and application to spring-back prediction. Int J Plast 29:13–41

36. Lee MG, Kim DY, Kim CM, Wenner ML, Wagoner RH, Chung K (2007) A practical two-surface plasticity model and its application to spring-back prediction. Int J Plast 23:1189–1212

37. Xue X, Liao J, Vincze G, Barlat F (2015) Twist springback characteristics of dual-phase steel sheet after non-symmetric deep drawing. Int J Mater Form . doi:10.1007/s12289-015-1275-2In press

38. Rauch EF (1998) Plastic anisotropy of sheet metals determined by simple shear tests. Mater Sci Eng A 241:179–183

39. Vincze G (2007) Investigation methodologies for metals used in forming processes. PhD. Dissertation. University of Aveiro, Portugal

40. Yoon JW, Barlat F (2006) Modeling and simulation of the forming of aluminum sheet alloys. ASM Handbook, Metalworking: Sheet Forming 14B:792–826

41. Rauch EF, Gracio J, Barlat F (2007) Working-hardening model for polycrystalline metals under strain reversal at large strains. Acta Mater 55:2939–2948

42. Martins PAF, Kwiatkowski L, Franzen V, Tekkaya AE, Kleiner M (2009) Single point incremental forming of polymers. Cirp Ann Manuf Techn 58:229–232